Obstacle Avoidance in R^n Based on Artificial Harmonic Potential Fields

Jürgen Guldner[1], *Vadim I. Utkin*[2], *Hideki Hashimoto*[3], *Fumio Harashima*[3]

[1]DLR, Inst. for Robotics & System Dynamics, Postfach 1116, D-82230 Wessling, Germany
[2]Dept. of Electrical Eng., The Ohio State Univ, 2015 Neil Ave, Columbus, OH 43210-1275, USA
[3]Univ. of Tokyo, Inst. for Industrial Science, 7-22-1 Roppongi, Minato-ku, Tokyo 106, Japan

Abstract

The artificial potential field method is frequently employed for obstacle avoidance both of mobile robots and of manipulator arms. This paper extends previous results for planar problems [1,2] to the general n-dimensional case. The complexity is reduced by projecting the n-dimensional workspace onto a 2D subspace called *operation plane*. Furthermore, only the closest obstacles are taken into account when designing the artificial potential field. Still, global convergence is achieved. The methodology is illustrated with several numerical examples.

1 Introduction

The desire to increase autonomy of robotic systems has posed the problem of on-line obstacle avoidance. For n-link manipulators, complexity of the obstacle avoidance problem in configuration space grows exponentially with n. An elegant approach for obstacle avoidance in $\mathbb{R}^n$ is the artificial potential field method, pioneered by Khatib [3] and studied by many others. The principle idea is to construct a suitable potential field with an attractive global minimum at the goal point and repulsive local maxima at the obstacles. In initial works, robot motion was guided by control forces acting along the gradient of the artificial potential field, implementing a dynamic relationship between the robot and its environment [4]. Obviously, this approach does not lead to tracking of the gradient. However, collision avoidance is guaranteed for potentials tending to infinity at obstacle boundaries, even in the face of bounded actuator resources [5].

Recently, sliding mode control was proposed to exactly track the gradient lines[3] [6,7]. The exact tracking capability opens completely new perspectives for artificial potential fields and allows direct design of gradients exhibiting desired characteristics [2].

In order to avoid the problem of local minima in potential fields, known to cause premature termination of robot motion at undesired locations [8,9], it was proposed in [6,7] to employ harmonic potential fields. Harmonic potentials $\mathcal{U}$ fulfill the Laplace equation $\nabla^T\nabla\mathcal{U} = 0$ [10]. Physical analogies can be found e.g. in electrostatics [6,7] and in dynamics of incompressible fluids [11]. For convenience, we will adopt electrostatics' terminology in the sequel, denoting singular points of the harmonic potential field as "point charges".

In recent [1,2], the *equilibrium point placement* method was introduced for designing harmonic potentials for planar problems. These works serve as a starting point for the present development and are recapitulated in the Section 2. The main contribution of this paper, generalization to problems of higher dimension, is discussed in Section 3. Illustrative numeric examples are shown in Section 4.

[3]The term "gradient lines" denotes trajectories $\dot{x} = \nabla U$ obtained when following the gradient ∇U of the potential U. However, explicit equations of the gradient lines do not have to be derived for obstacle avoidance using the artificial potential field method.

2 Planar Obstacle Avoidance

The workspace is assumed to contain an arbitrary number of nonintersecting obstacles at known locations. (For extension to unknown obstacles and perception based obstacle avoidance of mobile robots see [12].) Design of a suitable potential field was significantly simplified by the works of Rimon and Koditschek [5]. Given a set of diffeomorph mappings of star-shaped obstacle security zones into security circles, it suffices to concentrate on constructing a potential field for security circles.

2.1 Harmonic Potential Fields

Harmonic potentials $\mathcal{U}$ fulfill the Laplace equation $\nabla^T\nabla\mathcal{U} = 0$. Solution in $\mathbb{R}^2$ for $\vec{x} = (x_1, x_2)$ leads to the harmonic potential of a point charge q at

IEEE International Conference on Robotics and Automation
0-7803-1965-6/95 $4.00 ©1995 IEEE

$(0,0)$ [6,7,11] ($||\cdot||$ denotes the Euclidean norm)

$$\mathcal{U}(\vec{x}) = q \ln \frac{1}{||\vec{x}||} \quad (1)$$

The associated gradient is described by

$$\mathcal{E}(\vec{x}) = -\nabla \mathcal{U}(\vec{x}) = q \frac{\vec{x}}{||\vec{x}||^2}. \quad (2)$$

A description of the properties of harmonic potentials such as the superposition principle can be found, for example, in standard textbooks on partial differential equations.

2.2 Single Obstacle Case

A basic charge configuration for an obstacle security circle with radius R consists of a negative unit charge at the goal point in the origin and a positive charge $q < 1$ in the obstacle security circle center. The *equilibrium point placement* method [1,2] determines the obstacle charge to

$$q = \frac{R}{R+D}, \quad (3)$$

where D is the distance between the two charges. The resulting gradient field is shown in Figure 1.

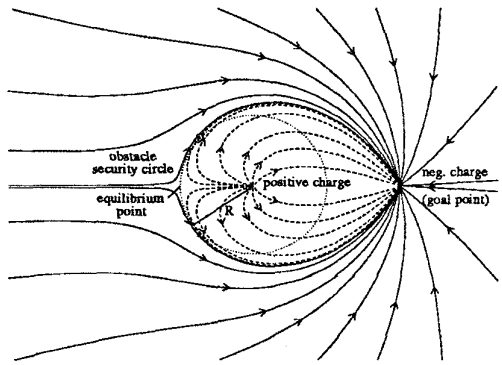

Figure 1: Gradient lines of a basic configuration with one pos. and one neg. charge

The gradient lines of the basic charge configuration exhibits two useful properties (for proofs see [1]):

- All gradient lines starting outside the circle (solid lines) remain outside.
- Following the gradient lines outside the circle continuously approaches the goal. (4)

The two properties ensure that the goal is always reached without penetrating into the obstacle security zone. At the unstable equilibrium point (see Figure 1), located on the boundary of security circle R (dashed line) opposite to the goal point, the curvature of the gradient lines tends to infinity. Hence tracking with constant speed is not possible with finite control resources. Two heuristics can be were proposed in [1,2] to preserve trackability. First, decreasing the velocity close to the singularity of the gradient. This may lead to an extremely slow approach towards the goal point for initial conditions close to the singular line through the two charges. The second heuristic remedies this problem by dynamically increasing the radius of the security circle in correspondence to the radial velocity component $\dot{x}_r$ directed towards the security circle center.

2.3 Multiple Obstacle Case

Multiple obstacles are each protected by nonoverlapping security zones, each with a separate transformation into a circle. By this assupmtion, a path to the goal always exists. In order to reduce computational efforts, only the closest obstacle is considered at each time instance. This requires to switch the potential field and the gradient lines whenever the robot crosses the equi-distance line[4]. Abrupt switching creates discontinuous gradient lines which cannot be tracked, see Figure 2 (a). The resulting oscillations are similar to those reported in [9]. To enable tracking of the gradient lines, the switching of the potential field from one obstacle to the next has to be smoothed. Within a boundary layer δ of $s_{equi} = 0$, both obstacles contribute to the overall potential with state-dependent or time-dependent weights [13]. In the example in Figure 2 (b), the weights depend linearly on the distance to the equi-distance line. Outside the boundary layer, still only the closest obstacle is considered. The two properties 4 of the gradient lines are preserved and global convergence is ensured [1,2].

3 Obstacle Avoidance in R^n

This section extends the results for planar obstacle avoidance to spaces of higher dimension $n > 2$. The concept of transforming star-shaped obstacle secu-

[4]The equi-distance line between two obstacles is the set of all points of equal distance to the security zones of these two obstacles and is denoted by $s_{equi} = 0$.

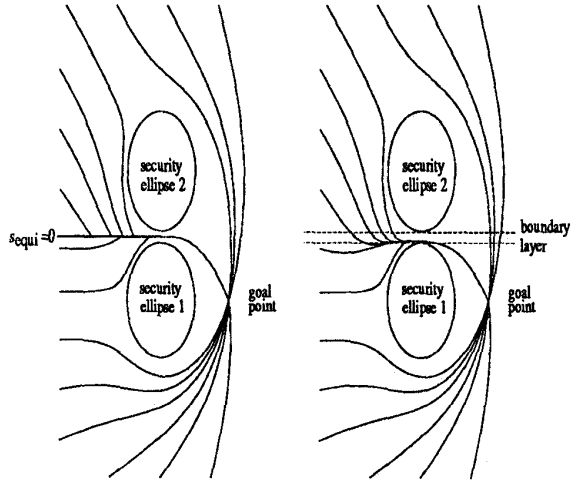

Figure 2: Gradient lines for two obstacles:
(a) Discontinuous gradient switching
(b) Smooth gradient switching

rity zones into security circles as used for the planar case in Section 2, is carried over to higher dimensions. It is beyond the scope of this paper to generalize the diffeomorph mappings given in [5] to $n > 2$ dimensions. The development in this paper concentrates on obstacle security zones modeled as spheres ($n = 3$) and hyper-spheres ($n > 3$).

An intuitive strategy would be to utilize a generalized solution of the Laplace equation for $\mathbb{R}^n$ [6]. However, to the best of the author's knowledge, no proof showing that the two properties of the planar gradient (4) also hold for higher dimensional potential fields, has been presented so far. We propose to continue to exploit the properties of the planar potential by projecting the n-dimensional problem into a subspace of dimension two.

3.1 Single Obstacle Case

In any space of dimension $n > 2$, three points uniquely define a subspace of dimension two. The goal point $\vec{x}_G \in \mathbb{R}^n$, the center of the obstacle security sphere (or hyper-sphere) $\vec{x}_S \in \mathbb{R}^n$, and the present robot location $\vec{x}_R \in \mathbb{R}^n$ are utilized to define the *operation plane* $\mathcal{P}$ as

$$\mathcal{P}(\vec{x}): \quad \vec{x} = \vec{x}_R + \alpha\vec{e}_1 + \beta\vec{e}_2, \quad \forall\, \alpha, \beta \in \mathbb{R} \quad (5)$$

where the vectors $\vec{e}_1 = \frac{\vec{x}_R - \vec{x}_G}{\|\vec{x}_R - \vec{x}_G\|}$ and $\vec{e}_2 = \frac{\vec{x}_R - \vec{x}_S}{\|\vec{x}_R - \vec{x}_S\|}$ have to be linearly independent. In the singular case when the three points $\vec{x}_G$, $\vec{x}_S$, and $\vec{x}_R$ lie in an one-dimensional subspace, the operation plane can be chosen with one degree of freedom. However, a small heuristic disturbance should be used to direct the robot away from this (unstable) singular one-dimensional subspace.

The operation plane $\mathcal{P}$ serves as a design platform. An n-dimensional obstacle security hyper-sphere with radius R reduces to an obstacle security circle with radius R on $\mathcal{P}$. Since we now again deal with a 2D problem of constructing an artificial potential field for a single obstacle security circle, the *equilibrium point placement* method presented in Section 2 can be applied directly. Choosing the present robot position as the origin of the coordinate system in the operation plane $\mathcal{P}$ further facilitates the computation. In fact, using a skew coordinate system, instead of a Cartesian coordinate system, with the coordinate axes being parallel to $\vec{e}_1$ and $\vec{e}_2$, the gradient can be found directly in $\mathbb{R}^n$ as

$$\begin{aligned} \mathcal{E} &= -\nabla(\mathcal{U}_G + \mathcal{U}_S) = \\ &= \frac{1}{\|\vec{x}_R - \vec{x}_G\|}\vec{e}_1 - \frac{q}{\|\vec{x}_R - \vec{x}_S\|}\vec{e}_2, \end{aligned} \quad (6)$$

where q is the obstacle charge chosen in (3).

The basic idea of the above approach is to restrict the motion to the operation plane $\mathcal{P}$ such that the properties of the planar potential field are preserved. This important simplification is made possible by the exact tracking property of the sliding mode controller [2, 6, 7].

3.2 Multiple Obstacle Case

In n-dimensional workspaces with several nonoverlapping obstacles, we propose to proceed in a similar fashion as in the planar case: Security spheres (or hyper-spheres for $n > 3$) are constructed for each obstacle. Only the closest hyper-sphere is regarded at any time instance. The operation plane and the associated potential field are found for each obstacle separately, as described above in Section 3.1.

In $\mathbb{R}^n$, switching of the potential field from one obstacle to the next can occur in subspaces of varying dimension. For illustration, consider a 3D situation. Between two obstacle security spheres exists a 2D equi-distance plane. Between three obstacles exist three 2D equi-distance planes for any two out of the three obstacles, and in addition one equi-distance line of dimension one to all three obstacles. In general n-dimensional space, points of equi-distance

to exactly k obstacles form $(n-k+1)$-dimensional subspaces $\mathcal{Q}_k^n$, for $2 \leq k \leq n$.[5]

The equi-distance hyperplanes partition the workspace into a number of regions with different gradients in each of them. Consider a situation where in each region adjecent to an $(n-k+1)$-dimensional equi-distance hyperplane $\mathcal{Q}_k^n$, motion converges to $\mathcal{Q}_k^n$ when following the respective gradient lines in each single region. In order to avoid discontinuous switching of the gradient from one obstacle to the next, smoothing of the gradient is proposed in a boundary zone $\mathcal{B}_k^n(\delta)$ of $\mathcal{Q}_k^n$ defined as

$$\mathcal{B}_k^n(\delta) \quad = \quad \{\vec{x} \in \mathbb{R}^n \mid \|\vec{x} \perp \mathcal{Q}_k^n\| \leq \delta\}, \qquad (7)$$

where $\|x \perp \mathcal{Q}_k^n\|$ denotes the length of the normal projection vector of $x \in \mathbb{R}^n$ onto $\mathcal{Q}_k^n$ and $\delta > 0$ is the width of the boundary layer. Within the boundary zone $\mathcal{B}_k^n(\delta)$, all k obstacles should contribute to the gradient with different weights. The respective weight μ_i of the repulsive potential $\mathcal{U}_{S_i}$ of obstacle i depends on the shortest distance d_i of the robot position to the equi-distance subspace $\mathcal{Q}_k^n$ determined by normal projection. Hence within $\mathcal{B}_k^n(\delta)$, the overall potential field $\mathcal{U}$ is given by

$$\mathcal{U} \quad = \quad \mathcal{U}_G + \sum_{i=1}^{k} (\mu_i \mathcal{U}_{S_i}), \qquad (8)$$

where for each of the ; $i = 1, 2, \ldots k$ obstacles being considered, a distance function is defined as

$$\mu_i = \frac{1}{k}\left(1 - \frac{1}{\delta}\left((k-1)d_i - \sum_{\ell=1, \ell \neq i}^{k} d_\ell\right)\right) \qquad (9)$$

When entering or leaving $\mathcal{B}_k^n(\delta)$, the derivative of each μ_i, $i = 1, 2, \ldots k$ is bounded. Inside the boundary layer $\mathcal{B}_k^n(\delta)$, the μ_i's depend linearly on the (continuous) distance functions d_i. Hence the μ_i's are continuous functions of the robot position and tracking of the gradient of $\mathcal{U}$ in (8) is possible with bounded control resources.

The width δ of the boundary zone has to be smaller than the shortest distance between any two obstacle security zones. The condition $\sum_{i=1}^{k} \mu_i = 1$ ensures that the properties of the gradient of the potential field for a single obstacle security zone, $\mathcal{E}_i = -\nabla \mathcal{U}_i = -\nabla(\mathcal{U}_G + \mathcal{U}_{S_i})$, are preserved for the overall potential field. Since $\mathcal{U}_G$ is common to all single obstacle potentials, $\mathcal{E} = -\nabla \mathcal{U}$ is a linear combination of k gradients $\mathcal{E}_i = -\nabla \mathcal{U}_i$, $i = 1, 2, \ldots k$ and forms a convex hull. Hence $\mathcal{E}$ is also contained in this convex hull and the resulting motion is confined to the boundary zone $\mathcal{B}_k^n(\delta)$ of the equi-distance subspace $\mathcal{Q}_k^n$. As a result, global convergence is guaranteed by the properties 4.

[5] In fact, for $n+1$ obstacles there also exists one point of common equi-distance. However, this point is unstable due to the "always-approaching-the-goal-point" property of the planar gradient field.

4 Illustrations

For convenient display, we present examples in 3D workspaces at the end of the paper. In most examples, the goal point is located in the origin of the coordinate system. The robot is modeled as a ball with point mass characteristics, and is depicted in time intervals ΔT.

The first example features a situation with a single obstacle security sphere and also depicts the operation plane $\mathcal{P}$. Exact tracking by sliding mode control [2, 6, 7] guarantees that the plane $\mathcal{P}$ is not left throughout the entire operation.

The second example in Figures 4 and 5 illustrates the varying number of obstacles being considered when moving through a workspace containing three obstacles. The obstacles are placed symmetric to the coordinate axis for convenient reference. Figure 5 depicts the respective distances to the obstacles. In the lower part of the graph, the obstacles considered concurrently are noted.

The last example illustrates application to a three-link revolute manipulator operating in an environment obstructed by two cylindrical blocks. The home position (0, 0, 0) is "arm straight up". In the simulation, motion from $(-\frac{\pi}{2}, \frac{\pi}{2}, \frac{\pi}{2})$ to $(\frac{\pi}{2}, \frac{\pi}{2}, \frac{\pi}{2})$ was commanded. The configuration space was generated off-line. For each of the three configuration space obstacles, a separate security ellisoid was constructed such that the entire obstacle was included. The trajectory in 3D configuration space is shown in Figure 6 with the base revolution θ_1 depicted along the x-axis, the upper-arm revolution θ_2-axis depicted along the y-axis, and the lower-arm revolution θ_3-axis depicted along the z-axis. The actual motion of the manipulator is depicted in nine snapshots in Figure 7.

5 Conclusions

This paper generalized previous results for planar obstacle avoidance of robots to $n > 2$ dimensions. Obstacles were protected by nonoverlapping sphe-

rical, or hyper-spherical, security zones. The problem was projected onto a 2D subspace. An *harmonic* artificial potential field was designed in this 2D subspace such that the gradient lines do not intersect the obstacle security zones, and furthermore continuously approach the goal point. Only the closest obstacle was taken in account when designing the potential field. Switching between potentials of different obstacles was smoothed to allow continued tracking of the gradient lines while preserving global convergence. The proposed method has a low complexity since the artificial potential field is designed in 2D and only few obstacles are considered concurrently. Numeric examples were used to illustrate the methodology of the proposed obstacle avoidance algorithm.

Acknowledgements

Jürgen Guldner appreciates the support from DAAD, German Acedemic Exchange Council, for visiting University of Tokyo, Japan in summer 1994. Vadim I. Utkin is grateful to Toshiba Co. for supporting this research during his stay at University of Tokyo, Japan, in 1994. The authors are thankful to Prof. Ackermann of DLR, Germany, for his continued encouragement of their joint research. The authors would like to thank the reviewer for their very heplful comments.

References

[1] J. Guldner and V. I. Utkin, "Sliding mode control for an obstacle avoidance strategy based on an electrical potential field," in *Proc. IEEE Conf. Decision and Control*, (San Antonio, TX, USA), pp. 424–429, 1993.

[2] J. Guldner and V. I. Utkin, "Sliding mode control for gradient tracking and robot navigation using artificial potential fields," *IEEE Trans. on Robotics and Automation, to appear*, 1995.

[3] O. Khatib, "Real-time obstacle avoidance for manipulators and mobile robots," *Int. Journal of Robotics Research*, vol. 5, no. 1, pp. 90–98, 1986.

[4] N. Hogan, "Impedance control: An approach to manipulation: Parts I-III," *ASME Journal of Dynamic Systems, Measurement and Control*, vol. 107, pp. 1–24, 1985.

[5] E. Rimon and D. E. Koditschek, "Exact robot navigation using artificial potential functions," *IEEE Trans. on Robotics and Automation*, vol. 8, no. 5, pp. 501–518, 1992.

[6] V. I. Utkin, S. Drakunov, H. Hashimoto, and F. Harashima, "Robot path obstacle avoidance control via sliding mode approach," in *Proc. IEEE/RSJ Int. Workshop on Intelligent Robots and Systems*, (Osaka, Japan), pp. 1287–1290, 1991.

[7] H. Hashimoto, F. Harashima, V. I. Utkin, S. A. Krasnova, and I. M. Kaliko, "Sliding mode control and potential fields in obstacle avoidance," in *Proc. European Control Conf.*, (Groningen, The Netherlands), pp. 859–862, 1993.

[8] P. Khosla and R. Volpe, "Superquadratic artificial potentials for obstacle avoidance and approach," in *Proc. IEEE Conf. on Robotics and Automation*, (Philadelphia, PA, USA), pp. 1778–1784, 1988.

[9] Y. Koren and J. Bornestein, "Potential field methods and their inherent limitations for mobile robot navigation," in *Proc. IEEE Conf. on Robotics and Automation*, (Sacramento, CA, USA), pp. 1398–1404, 1991.

[10] C. I. Connolly, J. B. Burns, and R. Weiss, "Path planning using Laplace's equation," in *Proc. IEEE Conf. on Robotics and Automation*, (Cincinati, OH, USA), pp. 2102–2106, 1990.

[11] J.-O. Kim and P. Khosla, "Real-time obstacle avoidance using harmonic potential functions," in *Proc. IEEE Conf. on Robotics and Automation*, (Sacramento, CA, USA), pp. 790–796, 1991.

[12] J. Guldner, V. I. Utkin, and R. Bauer, "Mobile robots in complex environments: A three-layered hierarchical path control system," in *Proc. IEEE/RSJ Int. Conf. on Intelligent Robots and Systems*, (München, Germany), pp. 1891–1897, 1994.

[13] J. Guldner, V. I. Utkin, and R. Bauer, "On the navigation of mobile robots in narrow passages: A general framework based on sliding mode theory," in *Preprints IFAC Symp. on Robot Control*, (Capri, Italy), pp. 79–84, 1994.

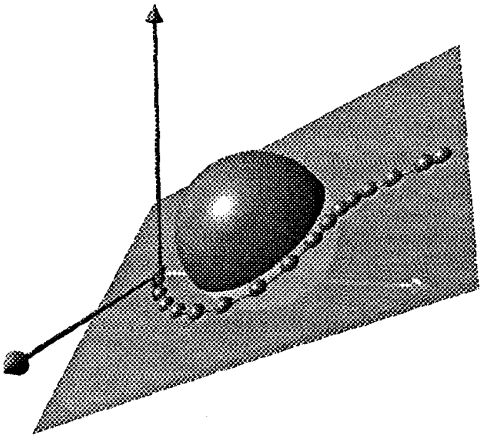

Figure 3: Operation plane for a single obstacle

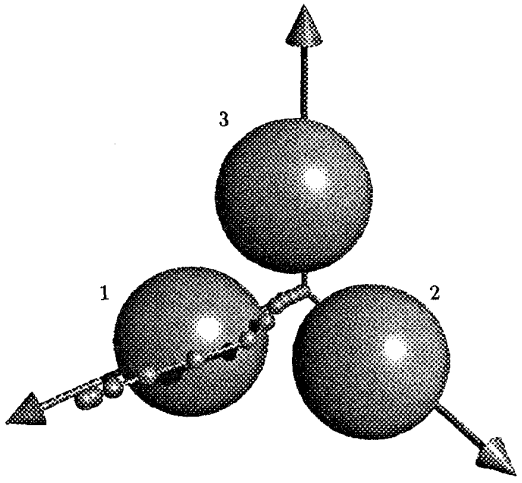

Figure 4: Workspace with three obstacles: motion trajectory

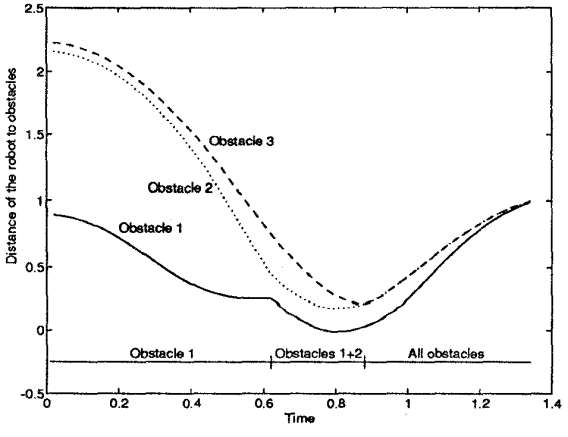

Figure 5: Workspace with three obstacles: obstacles being considered concurrently

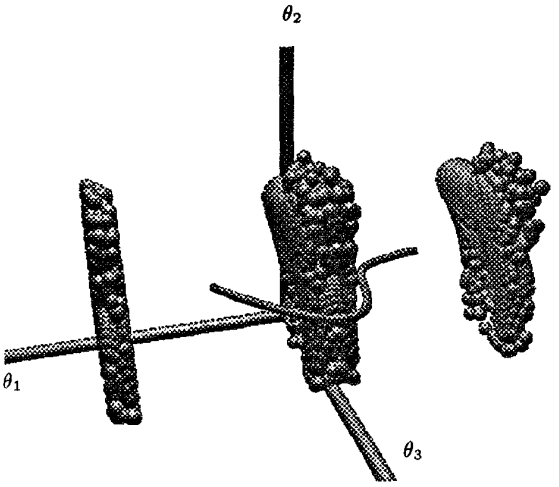

Figure 6: Motion trajectory of the 3-link manipulator in configuration space

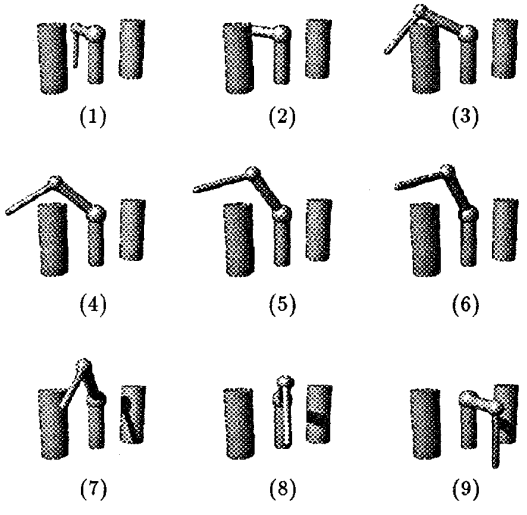

Figure 7: Motion trajectory of the 3-link manipulatorin the actual workspace